Effects of Nanometer Thick Passivation Layers on the Mechanical Response of Thin Gold Films

Bart C. Prorok and Horacio D. Espinosa

Department of Mechanical Engineering, Northwestern University, Evanston, Illinois 60208-3111, USA

The mechanical behavior of freestanding gold membranes 0.5 µm thick with and with out passivation layers was studied with the Membrane Deflection Experiment (MDE). Membrane width was varied from 2.5 to 20 µm to investigate size effects. The presence of the passivation layer had the effect of reducing the membrane strength. Yield stress, as well as fracture strain and stress, were all found to be significantly lower for the passivated specimens. The residual stress state was found to be significantly larger with passivation, to the degree of generating pre-stressed cracks at micromachined notches. The effect of membrane width had the greatest effect on the residual stress state with smaller widths having larger residual stress.

INTRODUCTION

Thin films have long been harvested by the microelectronic industry for their unique properties. Conventional thinking has usually categorized their electrical properties as the property of primary importance. In the past decade and a half though, other non-electronic properties such as chemical and mechanical have been found to also have great significance.[1-3] Mechanical properties in particular are critical when concerned with the

Submitted to the Journal of Nanoscience and Nanotechnology, 2001.

fact that devices must have structural integrity and also be reliable throughout their life expectancy.

In the extensive use of thin films in the microelectronic industry, particularly in CMOS (complementary metal-oxide semiconductor) transistors, a variety of materials are brought into contact with each other to create the unique function of the device, see Figure 1. Typically, these materials have considerably different electrical, mechanical, and thermal properties as well as different crystal structures and chemical affinity. When sandwiched together in a structure, interactions between them such as lattice and thermal expansion mismatches can have resounding effects on their properties. For instance, induced strains distort the lattice and thus can modify important semiconductor parameters such as the bandgap, effective masses of holes and electrons, and carrier mobility.[4-6] These effects come from either underlying substrate layers or overlying passivation or "capping" layers. The passivation layers may serve as a functional element of the device, a means to alter the lattice of the underlying layer, or simply as a barrier to reduce electromigration and other diffusion driven processes.[7]

CMOS structures are fabricated by depositing the thin film materials in patterns defined by photolithography. The variety of materials assembled to make the device typically have different deposition temperatures and thermal expansion coefficients. Existing layers may shrink or expand during deposition of overlying layers. Non-uniformities in microstructure and film thickness also exist. These effects all give rise to stresses in the

layers, the strength of which is a function of their susceptibility to these effects from the underlying and capping layers.

Stress and strain inside the films can result in the formation of misfit dislocations if the film is sufficiently thick.[4,8-12] The formation and density of dislocations are important in tailoring electronic properties of some devices.[13-17] However, there are also cases where the presence of dislocations and their ability to move under the influence of stress can have deleterious effects that lead to device failure.[1-3] Several scenarios of failure have been detailed by Nix.[1] Failure can occur by Hillock formation, cracking of the passivation layer through dislocation pile-up, and substrate cracking at geometrical stress concentrations.

Typically, the presence of substrate and passivation layers have a strengthening effect on the film, in that dislocation nucleation and motion are hindered by lattice distortions.[1,5,18] The dislocations that are formed are confined and can only move along the slip planes in the film. They will glide along these planes until they become pinned and or pile-up at the film interfaces. Also, the presence of a passivating layer obstructs dislocations from forming steps when they reach the surface.[19] The stress applied to the film must be at a critical level in order for these processes to occur.[20] A model developed by Freund[21-23] relates dislocation motion to this critically necessarily stress level. In considering the motion of a single dislocation in the film Freund found that the shear stress needed to drive a dislocation in a passivated film was 1.75 times that required to drive the same

dislocation in an unpassivated film. Similar strengthening behavior was observed in experimental studies.[7,24-29]

It is clear that a thorough understanding of the mechanical properties of passivated thin films is needed even in the case of an embedded layer whose only function is electronic in nature. In this paper we study the effect of passivation layers on plasticity and fracture of thin gold films. We use an experimental approach developed by Espinosa and co-workers.[30-34] Freestanding membranes were fabricated, using surface and bulk micromachining processes, with passivation layers of SiO_2 grown on either side. The membranes are in a fixed-fixed configuration spanning a specially micro-machined window. A Membrane Deflection Experiment (MDE) was used to achieve uniform direct tensile testing on the films in the absence of strain gradients.[30-34] The test identifies film residual stress, Young's modulus, onset of plasticity, and fracture stress.

EXPERIMENTAL PROCEDURE

Specially designed thin film Au specimens were microfabricated on (100) Si wafers. Specimen shape was defined on the top-side by photolithography and lift off. On the bottom side windows were etched through the wafer, underneath the specimens, with the purpose of creating suspend membranes. The passivation layers were grown on both sides of the gold membrane through sputtering deposition. The geometry of the suspended thin-film membranes can be described best as a double dog-bone tensile specimen. A more detailed description of their fabrication and shape is given in Espinosa

et al.[32] Figure 2(a) shows an optical image of the Au membranes. Membrane width was varied in each die, to examine size effects, while preserving the ratio length/width. This geometry was chosen to minimize stress concentrations and boundary-bending effects. Dimensions of four differently sized membranes can be described by their characteristic widths, W, of 2.5, 5, 10 and 20 um.

The Membrane Deflection Experiment (MDE) was used to achieve direct tensile stressing of the specimens.[32-34] The procedure involves applying a line-load, with a nanoindenter, at the center of the spanning membrane. Simultaneously, an interferometer focused on the bottom side of the membrane records the deflection. The result is direct tension in the gauged regions of the membrane with load and deflection being measured independently.

The data directly obtained from the MDE test must then be reduced to arrive at a stress-strain signature for the membrane. The load in the plane of the membrane is found as a component of the vertical nanoindenter load by the following equation:

$$\tan \theta = \frac{\Delta}{L_M} \quad \text{and} \quad P_M = \frac{P_V}{2 \sin \theta}, \tag{1}$$

where (from Figure 2b) θ is the angle of deflection, Δ is the displacement, L_M is the membrane half-length, P_M is the load in the plane of the membrane, and P_V is the load measured by the nanoindenter. Once P_M is obtained the Cauchy stress, $\sigma(t)$, can be computed from:

$$\boldsymbol{s}(t) = \frac{P_M}{A}, \tag{2}$$

where A is the cross-sectional area of the membrane in the gauge region. The cross-sectional area dimensions were measured using an Atomic Force Microscope (AFM).

The interferometer yields vertical displacement information in the form of monochromatic images taken at periodic intervals. The relationship between the distance between fringes, δ, is related through the wavelength of the monochromatic light used. Assuming that the membrane is deforming uniformly along its gage length, the relative deflection between two points can be calculated, independently of the nanoindenter measurements, by counting the total number of fringes and multiplying by $\lambda/2$. Normally part of the membrane is out of the focal plane and thus all fringes cannot be counted. By finding the average distance between the number of fringes that are in the focal plane of the interferometer, an overall strain, $\varepsilon(t)$, for the membrane can be computed from the following relation,

$$\boldsymbol{e}(t) = \frac{\sqrt{\boldsymbol{d}^2 + (\boldsymbol{l}/2)^2}}{\boldsymbol{d}} - 1. \tag{3}$$

This relationship is valid when deflections and angles are small. Large angles require a more comprehensive relation to account for the additional path length due to reflection

off of the deflected membrane. This task and further details are given by Espinosa et al.[32] For this study, deflection angles of all four membrane sizes are small and thus the above equation is used.

RESULTS AND DISCUSSION

Membrane Deflection Results

The microstructure of the 0.5 µm thick gold membranes consisted of equiaxed grains roughly 250-300 nm in diameter. Figure 3 is an SEM image of a membrane showing the top surface and side edge in the gauged region. It is clear from this image that 2-3 grains traverse the thickness of the film and several more across the width. The number of grains across the width can then be estimated as 4 to 6 times the width.

Gold membranes with and without passivation layers were deflected using the Membrane Deflection Experiment. A SiO_2 passivating layer was grown on both sides of the gold film. Film thickness was 0.5 µm for the gold and 30 nm for the passivated layers. Four different film widths were tested, 2.5, 5, 10 and 20 µm. Figures 4-7 are stress strain plots for membranes of these widths respectively. They compare the signatures of both passivated and unpassivated membranes. In order to directly compare the two signatures, compatibility issues must be considered in the passivated membranes. We assumed compatibility of deformation exists until membrane fracture. That is, both films, Au and SiO_2, remain intact and perfectly bonded with each carrying a portion of the applied load. The load carrying contribution from the passivation layers was then subtracted from the total load to obtain the response of only the gold film. This was accomplished by using a

Young's modulus for SiO_2 of 70 GPa. The formulae are: $P_M = P_{Au} + P_{SiO2}$; where P_M is measured and $P_{SiO2} = \varepsilon(t)E_{SiO2}$ with $\varepsilon(t)$ measured interferometrically.

Figure 4 shows the stress-strain results for the 2.5 µm width. Both the passivated (□) and unpassivated (◆) membranes have nearly identical Young's modulus, ≅ 54 GPa. It is clear from the plot inset that the passivated membrane has a higher state of residual stress. The extrapolation to zero strain of the elastic regions shows the passivated film has a residual stress of approximately 55 MPa while the unpassivated film has a residual stress of about 33 MPa. Yield stress was also found to vary from 125 to 220 MPa for the passivated and unpassivated membranes, respectively. Failure of the passivated membrane occurred at a much lower state of stress and strain then the unpassivated membrane. The significant dissimilarity of residual and yield stresses of the two membranes show that the passivation layer had considerable effect on membrane uni-axial strength.

Figure 5 shows the stress-strain results for the 5 µm width membrane. As with the 2.5 µm width membrane, both residual and yield stress of the two membranes were visibly different. The Young's modulus was nominal at 54 GPa for the unpassivated membrane and decreased slightly for the passivated membrane to 51 GPa. The reduction is small and within statistical variations to be expected from the small number of grains within the deformed volume. The residual stress increased from 33 to 45 MPa and the yield stress decreased from 170 to 133 MPa for the passivated film. Failure of the passivated membrane also occurred at a substantially reduced state of stress and strain.

Similar behavior also occurs for the membranes of larger width. Figures 6 and 7 are the stress-strain signatures of the 10 and 20 μm wide specimens, respectively. Young's modulus is consistent at ≅ 54 GPa for the unpassivated membranes and slightly decreased for the passivated membranes in the range of 49-50 GPa. Residual stress of the passivated membrane continues to be larger than the unpassivated membrane. In both specimen widths the residual stress values are in the regime of 28-30 MPa for the passivated membranes and 21-23 MPa for the unpassivated membranes. Yield stress for the 10 μm wide specimen decreased from 170 to 140 MPa with passivation. However, for the 20 μm wide specimen, the yield stress exhibited a drastic decrease from 140 to 52 MPa with passivation. In accordance with the behavior of the lesser widths, the larger widths failed under notably reduced states of stress and strain with passivation.

The reduction in Young's modulus for the three larger passivated films presents an enigma. Computational studies show that variations in Young's modulus can occur, due to statistical effects, when the number of grains through the width is below 1000.[35] However, extensive experiments conducted on unpassivated gold membranes,[32] did not exhibit the variations in Young's modulus highlighted here. It should be noted that at this size scale, it is difficult to determine if compatibility of deformation exists. In fact, the passivation layer may develop multiple cracks, as the composite film is continuously deformed. We have performed SEM and AFM observations of the tested membranes, after loading, and no evidence of multiple cracking was observed. In our opinion this does not totally rule out the possibility of multiple cracking in the SiO_2 films, but just the

inability to observe cracks that are closed or exhibit extremely small openings upon unloading. In-situ electron microscopy testing of freestanding films may be required to further elucidate the compatibility. Another more likely source of error is the assumed Young's modulus for the SiO_2 films. It is known that variations in E can result from deposition parameters and substrate effects.

The stress parameter data are summarized in Table 1 for all the membrane sizes. Several trends are apparent. First of all, it is clear that a size effect is governing the strength of the films. In previous work by the authors, on unpassivated films, specimen width was shown to significantly alter the stress-strain behavior of the membranes causing substantial changes in yield stress and fracture stress.[16] With this effect aside, the results reported in Table 1 clearly illustrate the influence of passivation on thin film mechanical behavior. The residual stress state noticeably increases and the yield stress significantly decreases for all specimen widths. The reduction in yield stress is accentuated when the width increases from 10 to 20 µm. Overall, the presence of the passivating layers reduced the strength of the membranes. Work by other researchers has yielded the opposite outcome.[1,5,24] However, their experimental techniques differed significantly from the Membrane Deflection Experiment. In all cases the passivated film was studied in the presence of and confined by a rigid substrate as well as strain gradients. The films were also only subjected to localized strains and stresses. The nature of the MDE test is such that the films are subjected to direct tensile testing with limited confinement and proportionally larger volumes of material subjected to uniform stresses. Thus, if a crack

forms in the passivation layer, it may act as a stress concentrator and cause the Au membrane to fail at lower than normal stress and strain levels.

Microstructural Observations

Figure 8 is an SEM image of a fracture in an unpassivated membrane 20 µm in width. Note that the specimen is at a 45° tilt. The fracture edge is rough and follows a random path across the width. Other observable features are ductile-like fingers in the stretching direction. In comparison to this, and shown if Figure 9, is an SEM image of a fracture for a passivated membrane 5 µm in width. Clearly visible on both sides of the membrane are the fracture edges of the SiO_2 passivation layer. They are highlighted with arrows in the figure. Note that they run directly perpendicular to the membrane's width. Protruding further out are the fracture surfaces of the gold film. They closely resemble the unpassivated edges, in that, they are rough and also contain ductile-like fingers. However, large plastic deformation of the gold seems to have been confined to this region where the passivation layer failed. All passivated membranes, regardless of width, failed by this manner.

Figure 10 shows SEM images of the fracture edges for an untested passivated membrane that failed during wafer handling. Identified by the white arrows on the right are areas where the passivation layer has delaminated from the gold at the fracture edge. The passivation layer is thin enough to allow some of the electrons to pass through and expose the gold fracture surface underneath. On the left side in the larger image are the

complementary edges where the passivation layer was stripped away. From this image, the passivation layer appears to indeed be a continuous film throughout the membrane.

The magnitude and effect of the residual stress in the membrane, as a result of the passivation layer, can be seen in Figure 11. The image shows an untested passivated membrane with a crack emanating from a notch. The notch was micromachined into the gold, prior to deposition of the passivation layer, to provide geometry conducive to studying the effect of stress concentrations. An examination of notches in numerous unpassivated membranes revealed no such cracks in any of the specimens. However, they were found to exist in most passivated membranes containing notches, particularly those of larger width. There is uncertainty though as to whether the crack exists only in the passivated layer or in the gold as well.

CONCLUSIONS

The MDE test was performed on freestanding gold films 0.5 μm thick both with and without 30 nm passivation layers of SiO_2 on each side. The membrane width was also varied from 2.5 to 20 μm to evaluate size effects. Results indicate that passivating the membrane's surfaces resulted in yield stress lower than unpassivated films of identical side for all membrane widths. Lower fracture strains and stresses and significantly larger states of residual stress were also found with passivation. Failure of the passivated membranes occurred where the passivating layer failed followed by localized plastic deformation of the gold confined to this region. The residual stress state of the passivated membranes was found to be large enough to generate cracks in untested membranes

where stress concentrations, such as micromachined notches, existed. The residual stress was also found to be larger for membranes of smaller width, following the same trend observed in unpassivated membranes.

The experiments reported here illustrate the need for the development of experimental techniques that can examine the atomic structure of the metal film as a function of the deformation while independently measuring force and stress. Such experiments are currently under development by Espinosa and Zhu[36] and are expected to provide valuable insight into failure mechanisms and failure evolution, as well as the regime in which compatibility of deformation exists. Likewise, theoretical analyses of the experiments are needed to understand the mechanisms responsible for the size and passivation effects reported here. In particular, defect types and structures consistent with the observed increase in film yield stress, as specimen width is reduced, need to be identified and quantified.

ACKNOWLEDGMENTS

This work was sponsored by the National Science Foundation under Career Award No. CMS-9624364 and the Office of Naval Research YIP through Award No. N00014-97-1-0550. Work was also supported in part by the Nanoscale Science and Engineering Initiative of the National Science Foundation under NSF Award Number EEC-0118025. Microscopy was carried out in the Center for Microanalysis of Materials, University of Illinois, which is partially supported by the U.S. Department of Energy under grant DEFG02-96-ER45439. Special thanks are due to G. Donahue and V. Diadiuk of the

Microsystems Technology Lab at the Massachusetts Institute of Technology for their aid in microfabrication and W. Oliver and B. Peters of MTS Systems Corporation for their assistance in the utilization of the nanoindenter during this investigation.

REFERENCES

1. W.D. Nix, Met. Trans. A, **20A**, 2217 (1989).
2. G.E. Henein and W.R. Wagner, J. Appl. Phys. **54**, 6395 (1983).
3. P.H. Townsend, D.M. Barnett, and T.A. Brunner, J. Appl. Phys., **62**, 4438 (1987).
4. S.C. Jain, *Germanium-Silicon Strained Layers and Heterostructures* (Academic Press, Boston, 1994).
5. S.C. Jain, A.H. Harker, and R.A. Cowley, Phil. Mag. A, **75**, 1461 (1997).
6. Y. Fu, S.C. Jain, M. Willander and J.J. Loferski, J. Appl. Phys., **74**, 402 (1993).
7. R.P. Vinci, E.M. Zielinski, and J.C. Bravman, Thin Solid Films **262**, 142 (1995).
8. J.H. ven der Merwe, J. Appl. Phys., **34**, 123 (1963).
9. J.W. Matthews and A.E. Blakeslee, J. Cryst. Growth, **27**, 118 (1974).
10. J.W. Matthews abd A.E. Blakeslee, J. Cryst. Growth, **29**, 273 (1975).
11. J.W. Matthews, *Epitaxial Growth* (Academic Press, New York , 1975).
12. D.Y. Baskov, M.Y. Gutkin, I.A. Ovid'ko, and A.G. Sheinerman, Mater. Phys. Mech., **2**, 10 (2000).
13. S.M. Sze,*High Speed Semiconductor Devices*, (Wiley Interscience, New York, 1990).
14. S.C. Jain and W. Hayes, Semicond. Sci. Technol., **6**, 547 (1991).
15. D.V. Morgan and R.H. Williams, Physics and Technology of Semiconductor Heterojunction Devices, (Peregrinus, London, 1991).
16. J.C. Bean, Proc. IEEE, **80**, 571 (1992).
17. R. People and J.C. Bean, Appl. Phys. Lett., **48**, 1338 (1986).
18. R. Bonnet, Phys. Stat. Sol. A, **177**, 219 (2000).
19. R. Venkatraman, S. Chen, and J.C. Bravman, J. Vac. Sci. Technol. A, **9**, 2536 (1991).
20. J.W. Matthews, S. Mader and T.B. Light, J. Appl. Phys., **41**, 3800 (1970).
21. L.B. Freund, J. Appl. Phys., **54**, 533 (1987).
22. L.B. Freund, J. Appl. Phys., **68**, 2073 (1990).

23. L.B. Freund, Adv. Appl. Mech., **30**, 1 (1994).

24. M.J. Kobrinski and C.V. Thompson, Appl. Phys. Lett. **73**, 2429 (1998).

25. T.S. Kuan and M. Murakami, Metall. Trans. A, **13**, 383 (1982).

26. A.J. Griffin, F.R. Brotzen, and C. Dunn, Scripta. Metall., 20, 1271 (1986).

27. M.F. Doerner, D.S. Gardner, and W.D. Nix, J. Mater. Res., **1**, 845 (1986).

28. M.F. Doerner, Ph.D. Dissertation, Stanford University, Stanford, CA (1987).

29. M.F. Doerner and S. Brennan, J. Appl. Phys., **63**, 126 (1988).

30. H.D. Espinosa, M. Fischer, Y. Zhu, and S. Lee, Proc. of the 4th Int. Conf. on Modeling and Simulation of Microsystems, M. Laudon and B. Romanowicz editors, 402 (2001).

31. H.D. Espinosa, B.C. Prorok, and M. Fischer, Proc. of the SEM Ann. Conf. on Experimental and Applied Mechanics, June 4-6, 2001, Portland, Oregon, 446 (2001).

32. H.D. Espinosa, B.C. Prorok, and M. Fisher, submitted to J. Mech. Phys. Solids. (2001).

33. H.D. Espinosa and B.C. Prorok, Proc. of the Symp. on Mech. Prop. of MEMS Structures, the 2001 Int. Mech. Eng. Congress in New York, New York, November 11-16 (2001).

34. H.D. Espinosa and B.C. Prorok, Mat. Res. Soc. Proc. **688**, 543 (2001).

35. R.L. Mullen, R. Ballarini, and Y. Yin, Acta Metal. Mater., **45**, 2247 (1997).

36. H.D. Espinosa and Y. Zhu, "Design of a MEMS device for in-situ TEM/SEM/AFM/STM testing of thin films, nanotubes and nanowires," http://clifton.mech.nwu.edu/~espinosa/projects_mn.html#tem, unpublished research (2001).

Table I. Summary of residual and yield stress results.

	Membrane Width							
	2.5 µm		5.0 µm		10.0 µm		20.0 µm	
	σ_r (Residual)	σ_y (Yield)	σ_r (Residual)	σ_y (Yield)	σ_r (Residual)	σ_y (Yield)	σ_r (Residual)	σ_y (Yield)
Passivated	55 MPa	125 MPa	45 MPa	133 MPa	30 MPa	140 MPa	28 MPa	52 MPa
Unpassivated	35 MPa	220 MPa	33 MPa	170 MPa	23 MPa	170 MPa	21 MPa	140 MPa

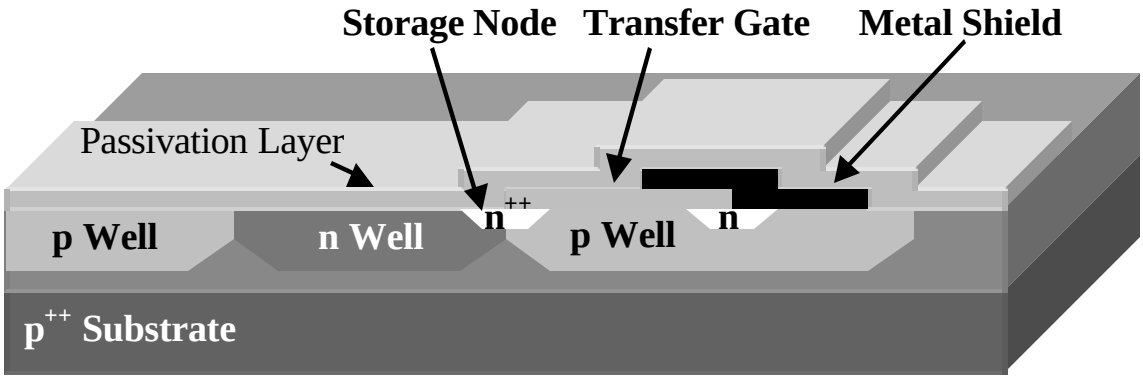

FIG. 1. Example of a CMOS device with multiple component layers and passivating layer.

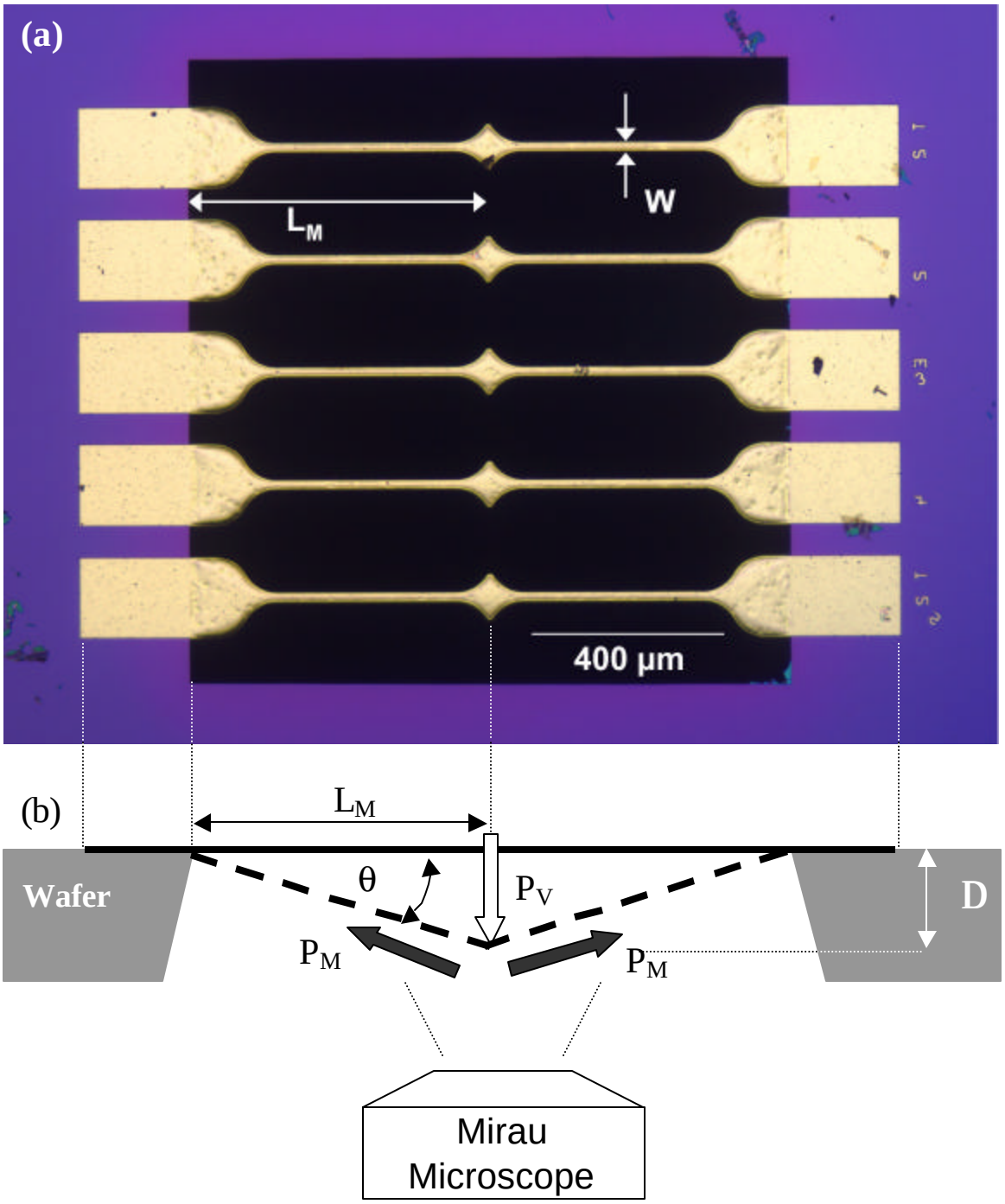

FIG. 2. (a) Optical image of Au membranes showing characteristic dimensions. L_M is half the membrane span, and W is the membrane width. (b) Side view of the MDE test showing vertical load being applied by the nanoindenter, P_V, the membrane in-plane load, P_M, and the position of the Mirau microscope objective.

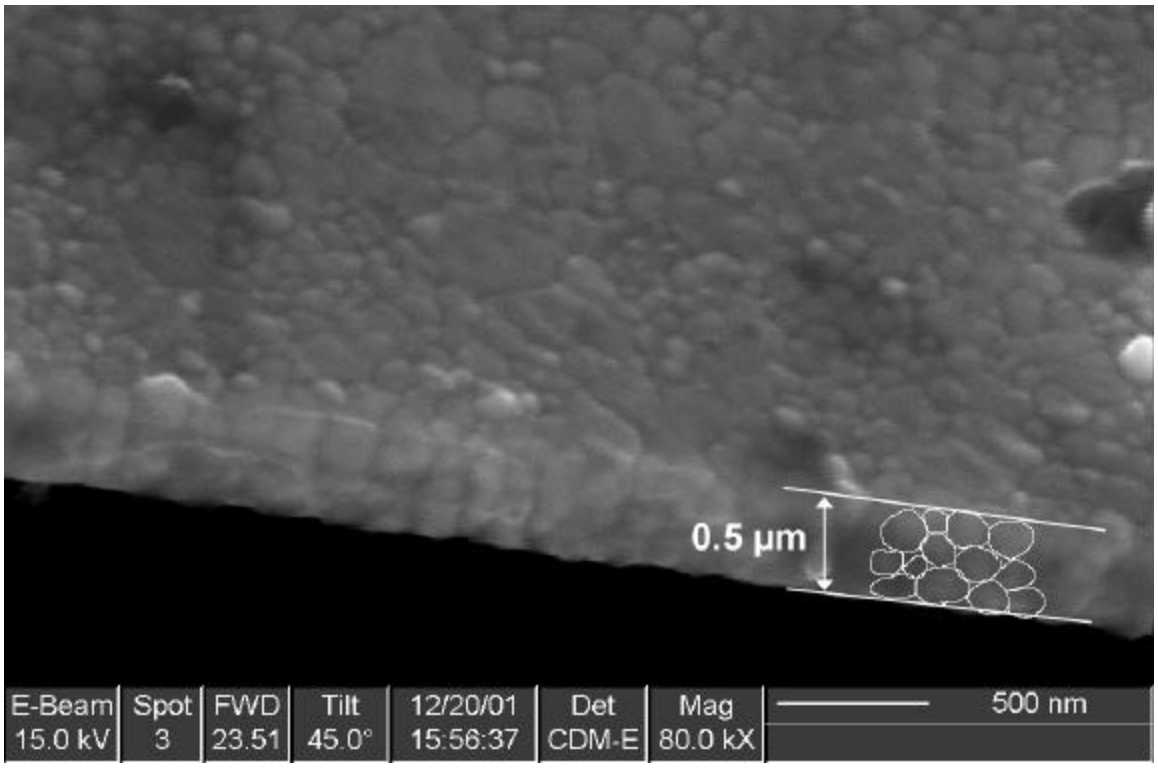

FIG. 3. SEM image of the longitudinal cross-section of an unpassivated membrane showing the microstructure through the thickness.

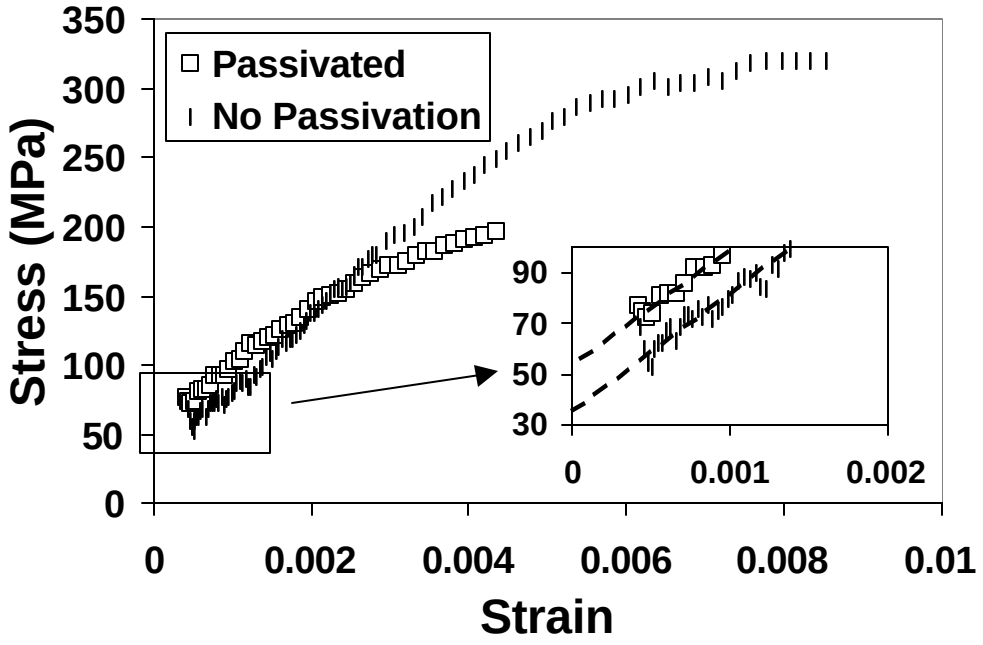

FIG. 4. Stress-strain results for passivated and unpassivated membranes 2.5 µm wide.

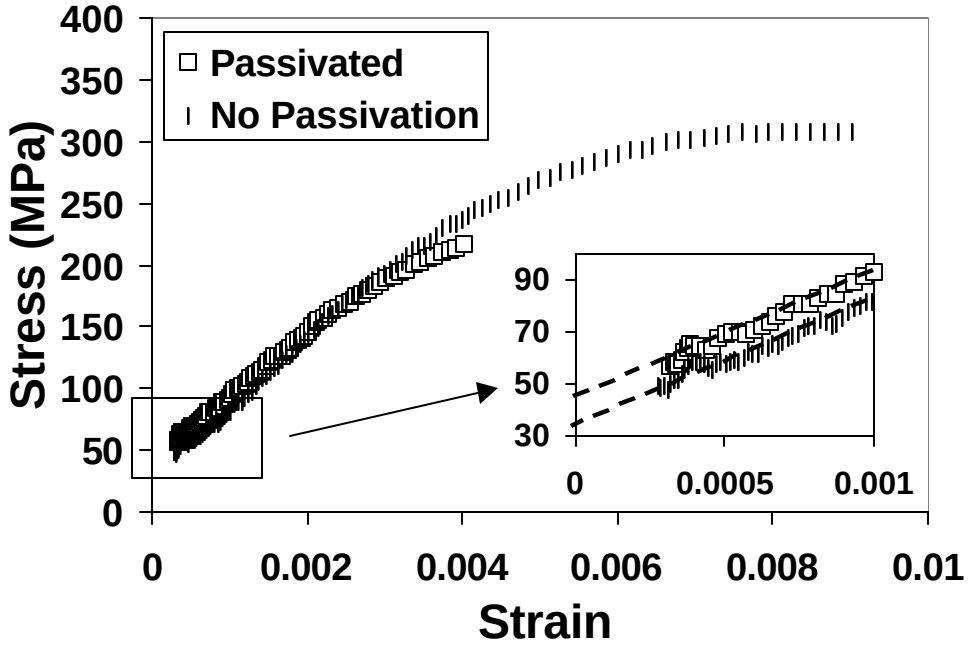

FIG. 5. Stress-strain results for passivated and unpassivated membranes 5.0 µm wide.

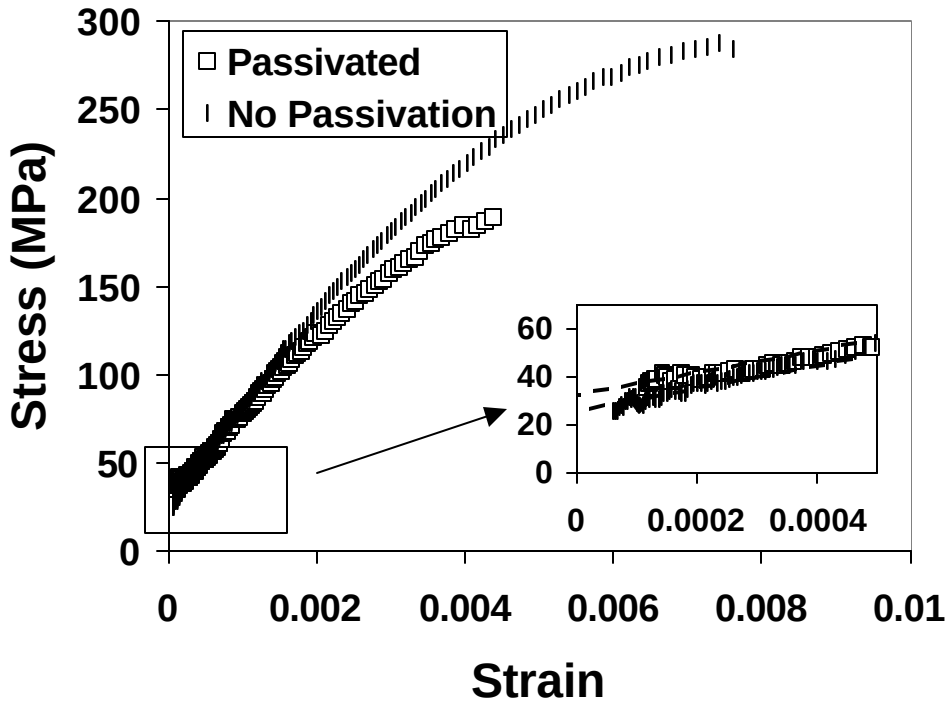

FIG. 6. Stress-strain results for passivated and unpassivated membranes 10.0 µm wide.

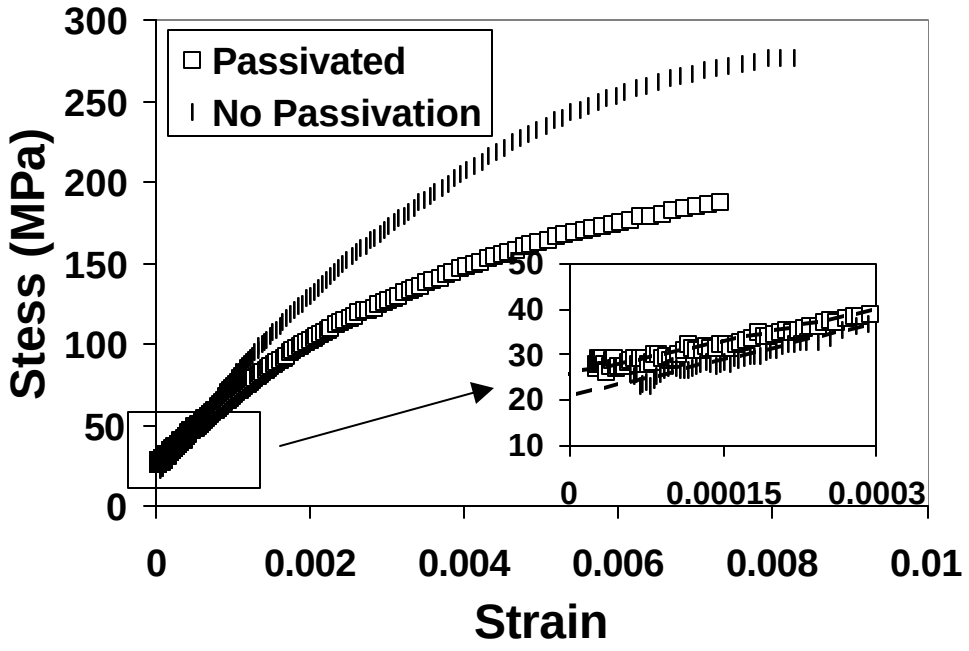

FIG. 7. Stress-strain results for passivated and unpassivated membranes 20.0 µm wide.

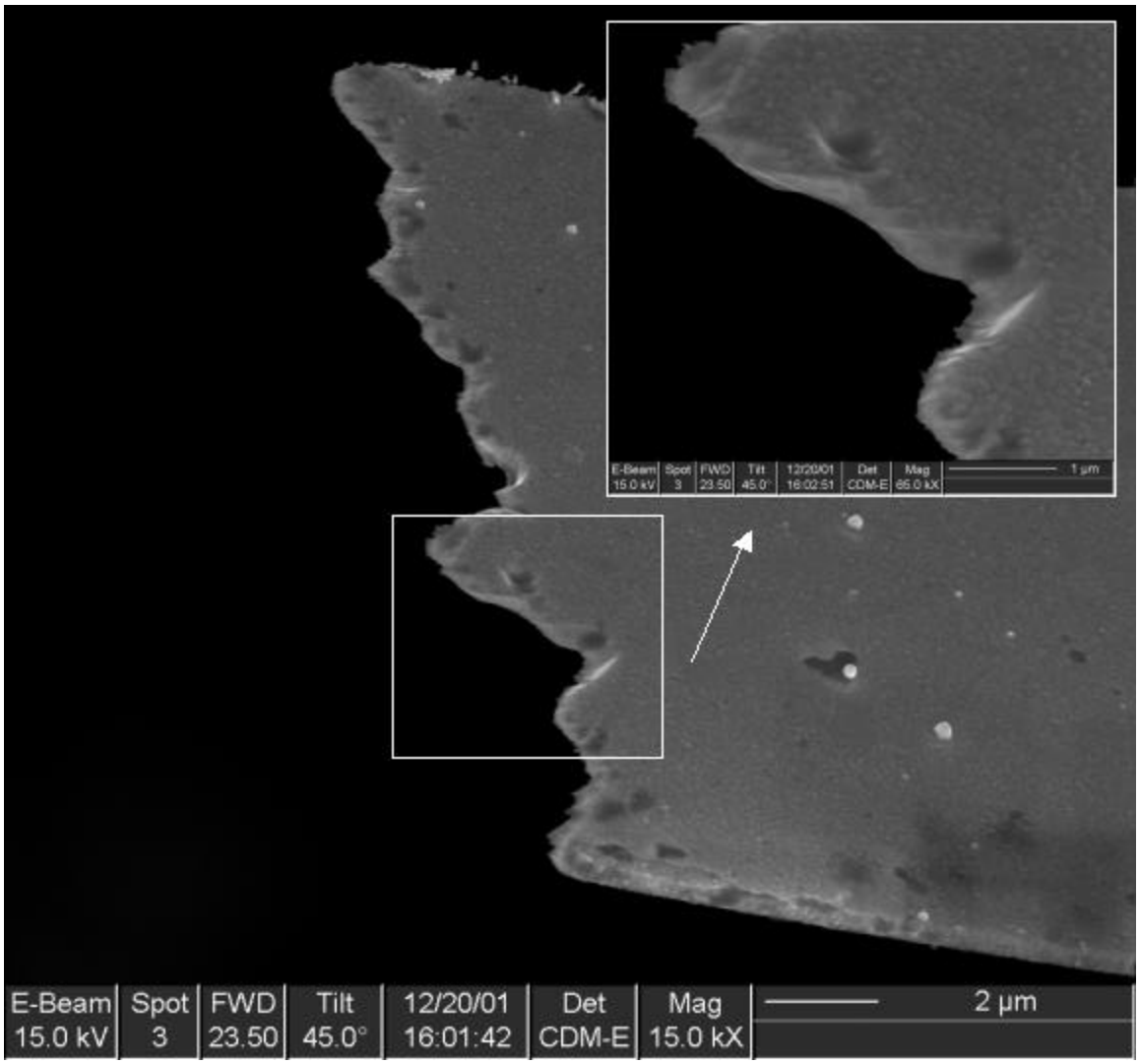

FIG. 8. SEM image of the fracture surface for the 20 µm wide unpassivated membrane.

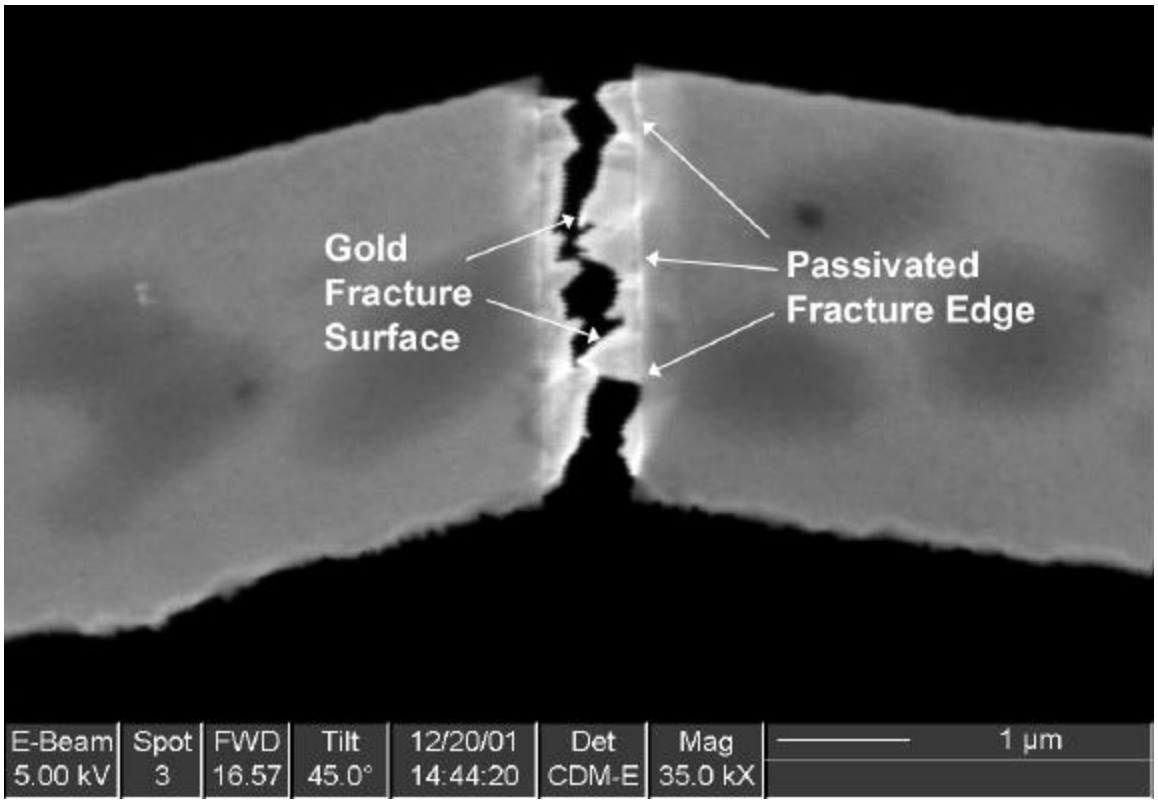

FIG. 9. SEM image of a fracture surface for the 2.5 µm wide passivated membrane.

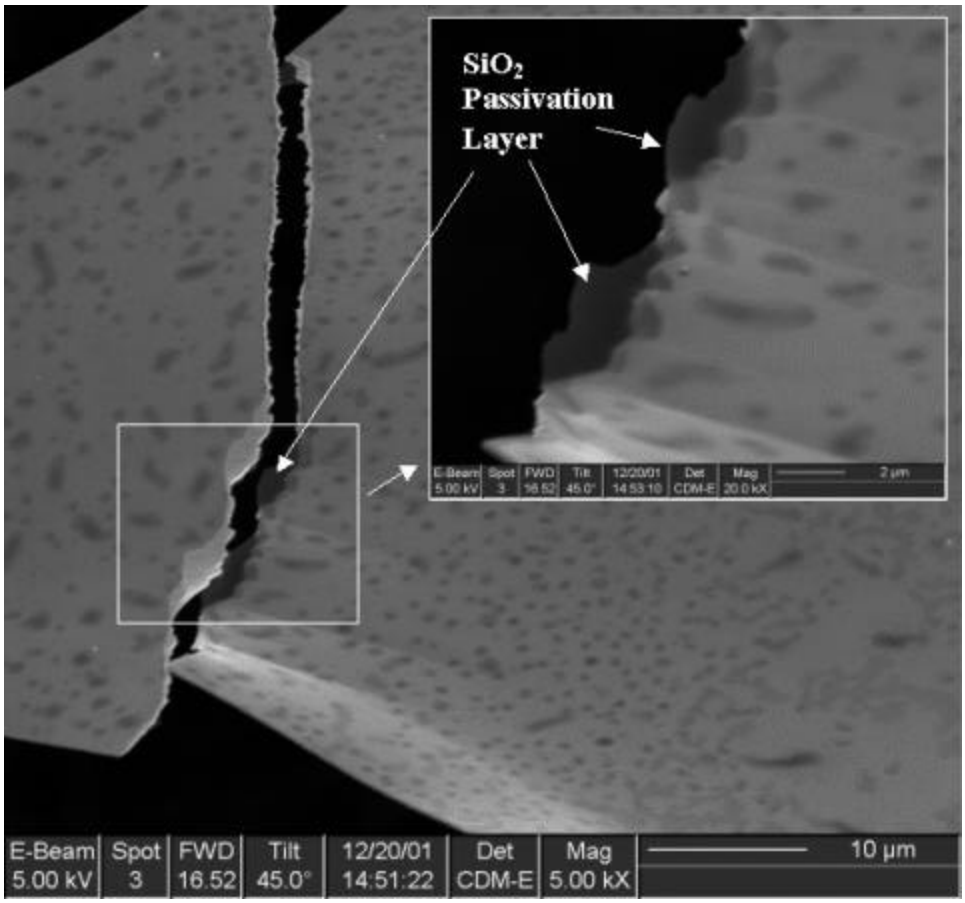

FIG. 10. SEM image of a passivated membrane showing delamination of the passivation layer near the fracture surface.

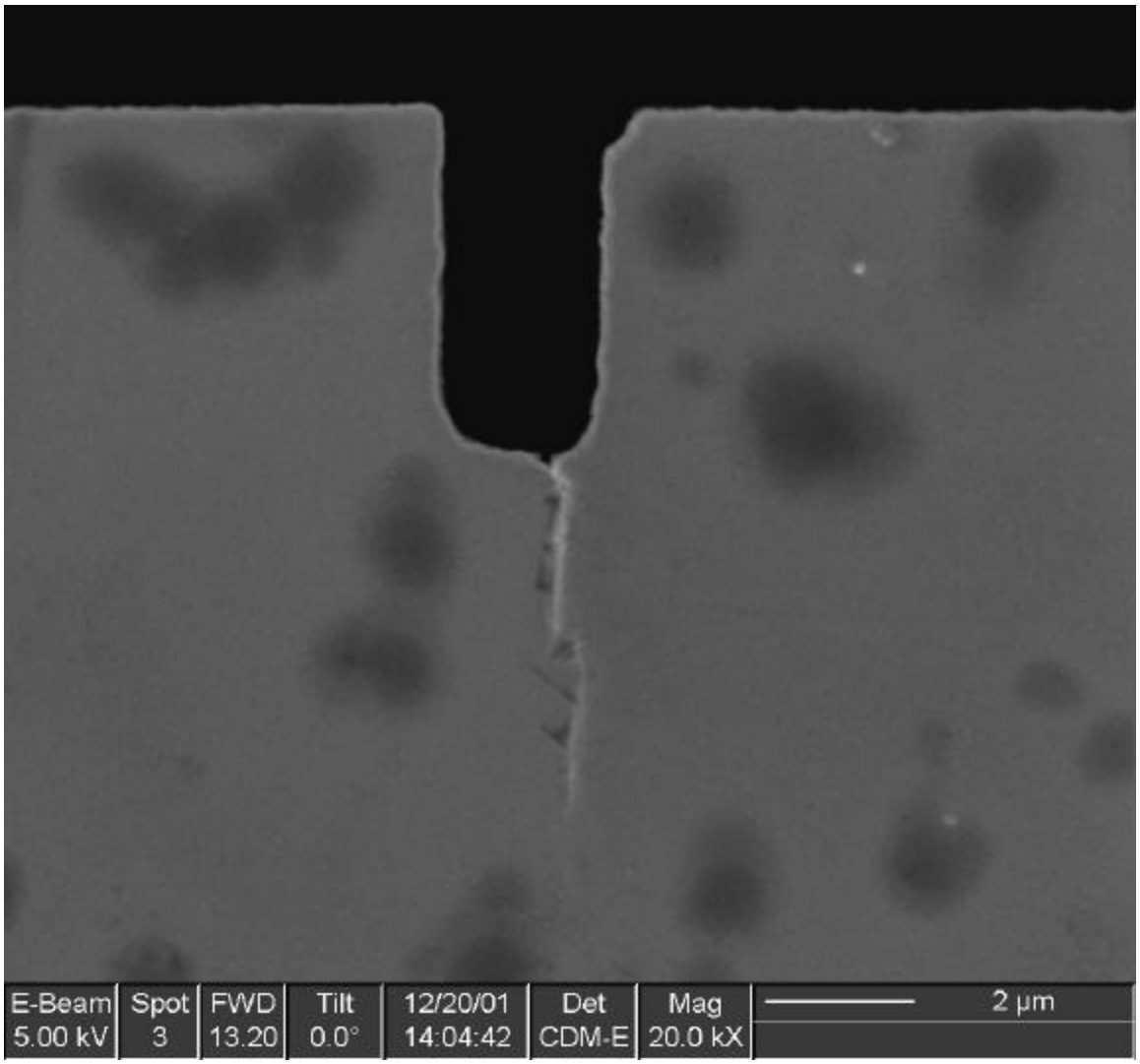

FIG. 11. SEM image of an untested passivated membrane showing a crack emanating from a micromachined notch.